



Chemical States, Structural, Electrical and Current Phenomenon Properties of a Au/Cobalt Phthalocyanine/Undoped-InP MPS-Type Diode with a CoPc Interlayer

A. Usha Rani¹ · V. Rajagopal Reddy¹ · C. Venkata Prasad¹ · A. Ashok Kumar²

Received: 17 February 2024 / Accepted: 23 March 2024

© The Author(s), under exclusive licence to Springer Science+Business Media, LLC, part of Springer Nature 2024

Abstract

This work reviews the impact of cobalt phthalocyanine (CoPc) interlayers on the electrical and current transport properties of Au/undoped-InP Schottky diodes (SDs). The crystalline quality of CoPc films was confirmed using dominant vibrational bands observed in Raman measurements. Using X-ray photoemission spectroscopy (XPS), the chemical properties were assessed and the results confirmed that the CoPc interfacial layer was deposited on undoped-InP (un-InP). The Au/CoPc/un-InP metal/polymer/semiconductor (MPS) diode showed a better rectification ratio than did the SD. The estimated barrier height (Φ_B) of the MPS diode (0.77 eV (I-V)) was greater than the SD (0.66 eV (I-V)), signifying that Φ_B was modified by a CoPc layer. Using Cheung's, and Norde methods and Ψ_s -V plots, the Φ_B , ideality factor and series resistance were assessed. The Φ_B values estimated by these techniques were well matched with one another demonstrating their constancy and validity. A lower density of states (N_{SS}) is attained for the MPS diode than for the SD, demonstrating that the CoPc layer reduced the N_{SS} . The forward log I-log V plot of both the SD and MPS suggests ohmic-type behavior and space charge limited current (SCLC) in the lower-bias and upper-bias regions. The Poole–Frenkel emission (PFE) is ruled at the lower-bias, while, the Schottky emission (SE) is governed in the upper-bias regions under reverse bias in both the SD and MPS diodes. The findings confirmed that the CoPc layer is a probable material for the construction of organic–inorganic devices.

Keywords CoPc · XPS · MPS diode · I-V · Series resistance · Density of states · Current transport process

1 Introduction

Metal–semiconductor (MS) junctions play an important role in the construction of electronic appliances because of their specific features, low voltage drop, fast switching, low tenancy space in integrated electronics, and minimal cost; additionally, MSs are utilized as Schottky barrier diodes in OLEDs, photovoltaic cells, OFETs, thermistors, switching and memory systems, organic solar cells and negative–resistance devices [1–4]. To fabricate these devices, indium phosphide (InP) is an exquisite semiconductor substance owing to its distinctive physical and electrical properties. Conversely,

it is difficult to reach a barrier height greater than 0.5 eV on an InP substrate because the surface Fermi level pinning increases as the occurrence of enormous surface states and different nonstoichiometric defects increases [5]. Thus, a high reverse leakage current is achieved due to the low barrier height of InP-based Schottky diodes, which results in poor electrical performance in the devices. To overcome this issue there may be several techniques available to modify and continuously manipulate the barrier height wherein organic/polymer interlayers are used between the metal and semiconductor [6–10]. The fabrication and characterization of MS junctions with organic/polymer interlayers are challenging issues in the research/scientific community.

Recently, the size of electronic devices has reached the molecular entity scale, as confirmed by the increasing attention given to the considerate transport of organic molecules associated with two metal contacts [11] and metal/organic or polymer MS junctions [6]. It is widely accepted that the interfacial layer (IL) established at the metal–semiconductor interface organizes the electrical features of Schottky

✉ V. Rajagopal Reddy
reddy_vrg@rediffmail.com

¹ Department of Physics, Sri Venkateswara University, Tirupati 517 502, India

² Department of Physics, Y.S.R. Engineering College of Yogi Vemana University, Proddatur 516 360, India

contacts. As a result, the evaluated barrier properties of the metal/IL/semiconductor contacts are better than those of traditional MS junctions, which may be attributed to the space-charge region of the semiconductor. Numerous investigations have shown that the barrier heights of MS junctions can be improved by the addition of organic or polymeric layers in the middle of metals and semiconductors [12–24].

Organic materials have attracted extensive attention for their use in molecular electronic and optoelectronic devices [13, 25]. In recent years, phthalocyanines created from organic materials have played a vital role in the manufacture of devices with organic molecules. Notably, cobalt phthalocyanine (CoPc) has semiconducting properties and is a metal phthalocyanine (MPc) that can be regularly employed in several organic electronic devices [26]. Furthermore, metal phthalocyanines are water and air-stable, thermally strong and harmless, and may be sublimed or sputtered with highly even films on different substrates. Metal phthalocyanines are also quite cheap and easy to prepare. In particular, CoPc can be used as a hole-injection layer, with considerable upgrades in turn-on voltage and luminance in OLEDs. Additionally, Kao et al. [27] confirmed the enhancement in the turn-on voltage and luminance in OLEDs with the use of the CoPc layer as a hole injection layer. CoPc may also be utilized to fabricate carbon-black-based electrocatalysts. Other advantages of organic materials over insulators or oxide materials include easy preparation, low cost and power ingesting, low weight, great mechanical stability, water-solubility and good charge storage capacity. Furthermore, the CoPc films on the InP substrate offer numerous advantages, including enhanced spin manipulation, improved photovoltaic performance, enhanced optoelectronic properties, versatile integration in multifunctional devices, and tunable magnetic sensitivity. Considering these notable characteristics of an organic interlayer (CoPc), in this work, Au/CoPc/un-InP metal/polymer/ semiconductor (MPS)-type Schottky diodes were prepared with a cobalt phthalocyanine interlayer. The overall performance and operating range of these junctions are associated with many issues including surface preparation, barrier height homogeneity and interlayer at the interface, surface state density (N_{SS}), shunt (R_{sh}) and series resistance (R_s), and applied bias potential, frequency and temperature [13, 16, 24]. Mainly, the interfacial layer, N_{SS} , R_{sh} , R_s and applied electric field/voltage are extra active in the performance of the junction. Current–voltage (I–V) measurements of the Au/CoPc/un-InP MPS diodes were performed and the barrier height, R_{sh} , R_s and N_{SS} were determined at room temperature. These derived parameters are correlated with the results of the Au/un-InP Schottky diode (SD) to assess the influence of the interlayer at the interface. Similarly, the conceivable forward and reverse

leakage transport processes of the Au/un-InP and Au/CoPc/un-InP MPS diodes are depicted and described.

2 Experimental Procedure

First, one side of a polished undoped-InP (un-InP) wafer (bought from Semiconductor Wafer, Inc., Taiwan) was cut into slices, after which the slices were gutted with warm organic solvents to eliminate impurities by ultrasonication for 5 min every step. Later, to remove the native oxide on the InP surface, the wafer was washed with dilute aqua regia $2\text{HNO}_3:2\text{HCl}:1\text{H}_2\text{O}$ for 3 min and dipped in DI water followed by drying with nitrogen gas. Then, the indium (In) was coated on the unpolished side of the wafer as an ohmic contact, subsequently, the contacts were annealed at $350\text{ }^\circ\text{C}$ for 1 min under ambient nitrogen. Then, cobalt phthalocyanine (CoPc) films were coated on the InP surface under a vacuum of $7\sim 8\times 10^{-6}$ mbar using a thermal evaporation approach. The CoPc film thickness was approximately 40 nm which was measured by a profilometer. Afterwards, gold (Au) Schottky junctions were prepared by an e-beam evaporation method with a 0.7 mm diameter on a CoPc film. The developed configuration was an Au/CoPc/un-InP metal/polymer/semiconductor (MPS) type Schottky diode. Furthermore, an Au/un-InP Schottky diode (SD) was prepared without the CoPc layer for comparison with the results of the MPS junction. The chemical states, structural and morphological properties of the CoPc/InP layers were studied using XPS, Raman and atomic force microscopy (AFM) measurements. The SD and MPS diodes were electrically measured through the current–voltage (I–V) approach by a Keithley 2400 source measuring unit.

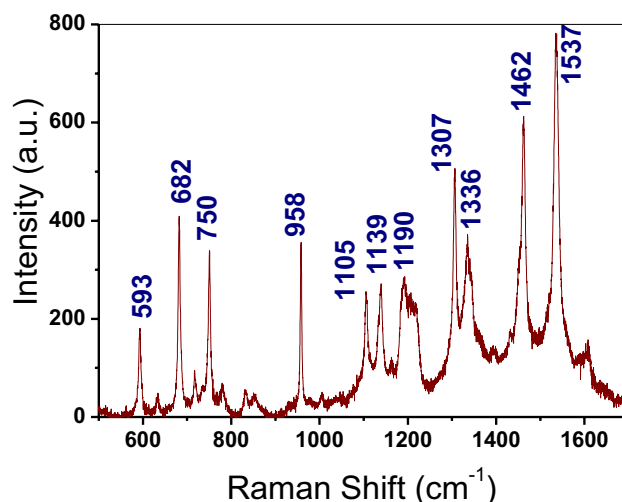


Fig. 1 Raman measurements of the CoPc films on a glass plate

3 Results and Discussion

The structural properties of CoPc films on quartz glass were analysed using Raman measurements. The Raman spectrum as shown in Fig. 1 was measured using an argon laser at an excitation wavelength of 488 nm in the range from 500 to 1700 cm^{-1} . The characteristic vibrational bands identified at 593 and 682 cm^{-1} correspond to C–N bond stretching (A_{1g} bond) due to benzene ring formation and C–C vibration, respectively, in the CoPc molecule [28, 29]. The vibrational band with the maximum intensity is observed at 1537 cm^{-1} and is correlated with the B_{1g} mode

and corresponds to the stretching of the C=N bond. The vibrational band observed at 1537 cm^{-1} signifies the crystalline quality of the CoPc compound [30].

The XPS survey spectrum of CoPc depicted in Fig. 2a, shows the presence of four elements: C 1s, N 1s, O 1s, and Co 2p, with the oxygen originating from the oxygen-containing groups within CoPc. The remaining elements are consistent with the elemental composition of CoPc. Figure 2b shows that the high-resolution C 1s spectra exhibited four peaks located at binding energies (BE) of 284 eV, 285.35 eV, 286.15 eV, and 287.25 eV, which are attributed to (C–C), (C=C), (C–O/C–N) and (C=O/C=N), respectively [31–37]. The N 1s spectrum presented in

Fig. 2 XPS spectra of the CoPc/InP interface: (a) survey spectra of CoPc, (b) C 1s, (c) N 1s, (d) Co 2p, (e) In 3d, and (f) P 2p

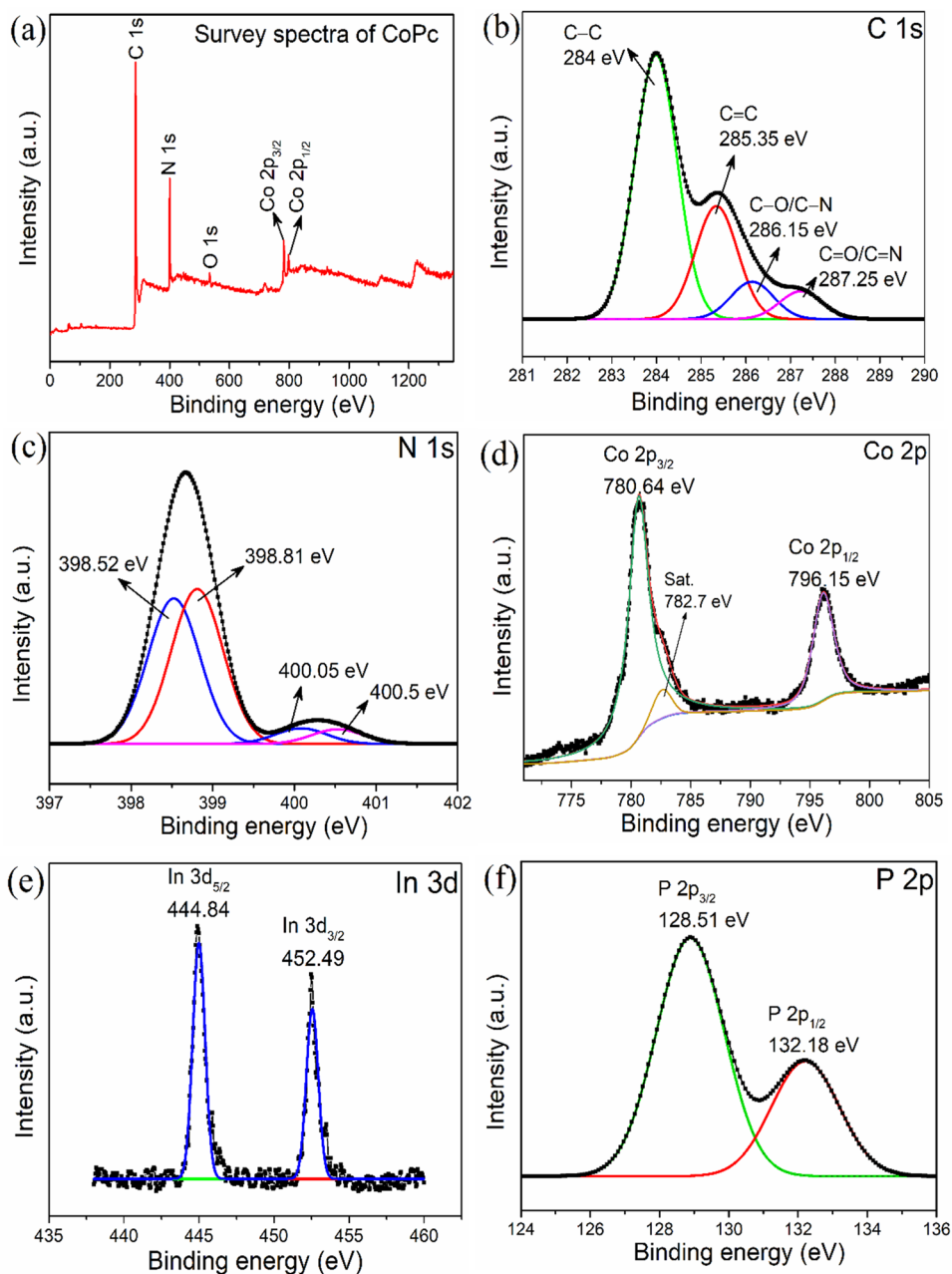


Fig. 3 (a) Outline of the Au/CoPc/un-InP MPS diode with a CoPc interlayer and (b) AFM image of the CoPc film on the un-InP surface

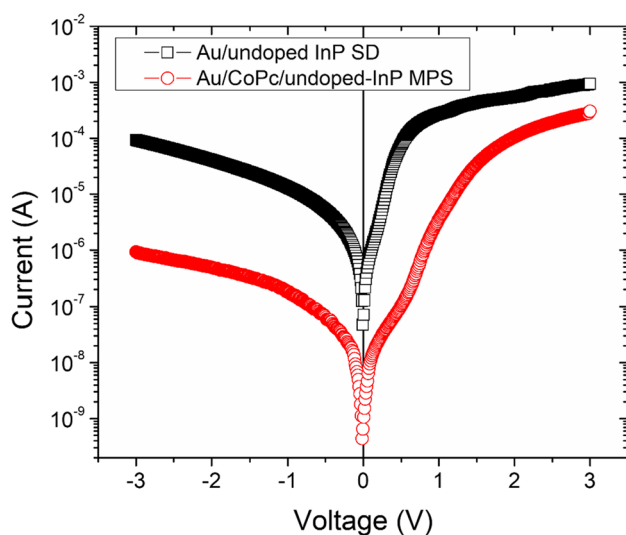
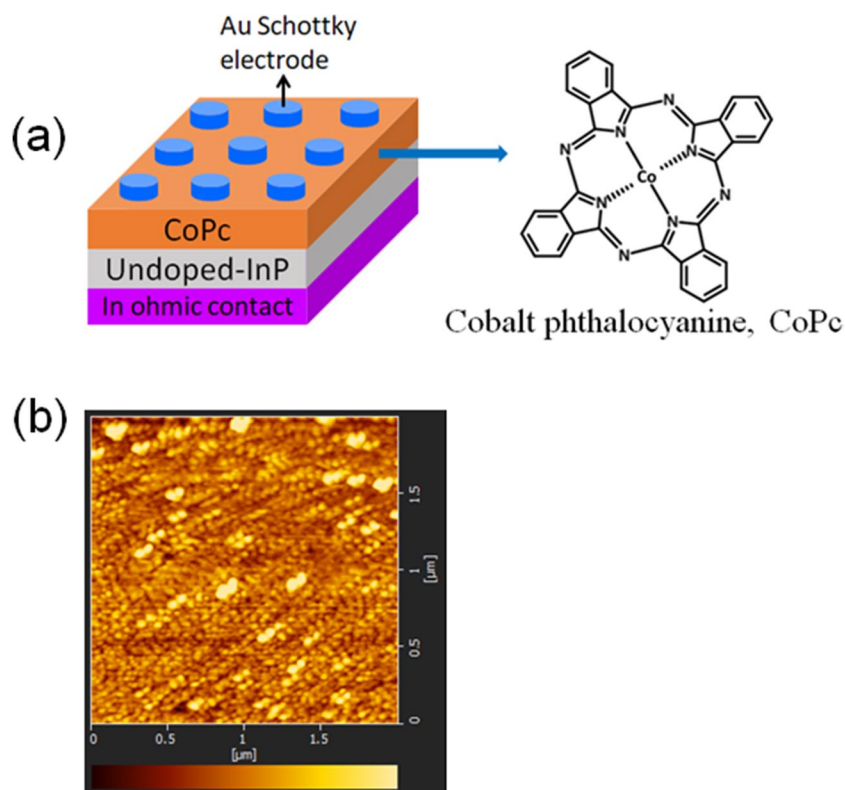


Fig. 4 Current–voltage (I–V) plot of the Au/un-InP SD and Au/CoPc/un-InP MPS diodes

Fig. 2c clearly shows four kinds of nitrogen. Specifically, the peaks located at BEs of 398.52 eV and 400.05 eV correspond to nitrogen atoms within the phthalocyanine ring, while the peak at a BE of 400.5 eV indicates the presence of an amide ($-\text{O}=\text{C}-\text{NH}$), confirming the success of the reaction between phthalocyanine and citric acid.

Additionally, the peak at a BE of 398.81 eV is ascribed to the coordination between cobalt and nitrogen [31, 35, 36]. Figure 2d shows the Co 2p spectra, two peaks are observed at BEs of 780.64 eV (its satellite peak at 782.7 eV) and 796.15 eV which are assigned to Co 2p_{3/2} and Co 2p_{1/2}, respectively [38]. Figure 2e illustrates the In 3d spectrum, where the 3d_{3/2} and 3d_{1/2} peaks are detected at BEs of 444.84 and 452.49 eV, respectively [39]. Figure 2f presents the high-resolution P 2p spectrum, which includes contributions. In particular, the 2p_{1/2} and 2p_{3/2} peaks are observed at BEs of 132.18 eV and 128.51 eV, respectively, indicating the presence of the phosphide (P^{-3}) [39, 40]. The results confirm that the CoPc is formed on the InP surface.

To assess the influence of the CoPc interlayer on the electronic features of the Au/undoped InP Schottky diode (SD), a Au/CoPc/un-InP metal/polymer/semiconductor (MPS)-type Schottky diode was fabricated and the outline sketch is shown in Fig. 3a. Figure 3b depicts the AFM topography of the thermally deposited CoPc films on the un-InP surface measured in the active area of $2\ \mu\text{m} \times 2\ \mu\text{m}$. The acquired RMS of the CoPc film is 4.499 nm, which suggests that the morphology of the CoPc film surface is noticeably smooth. Figure 4 depicts the I–V features of the Au/un-InP Schottky diode and Au/CoPc/un-InP MPS diode. A higher rectification ratio is obtained for the MPS diode (327) than for the SD (10) diode at a bias of 3 V.

Fig. 5 Plot of junction resistance (R_j) versus voltage (V) for the Au/un-InP SD and Au/CoPc/un-InP MPS diodes

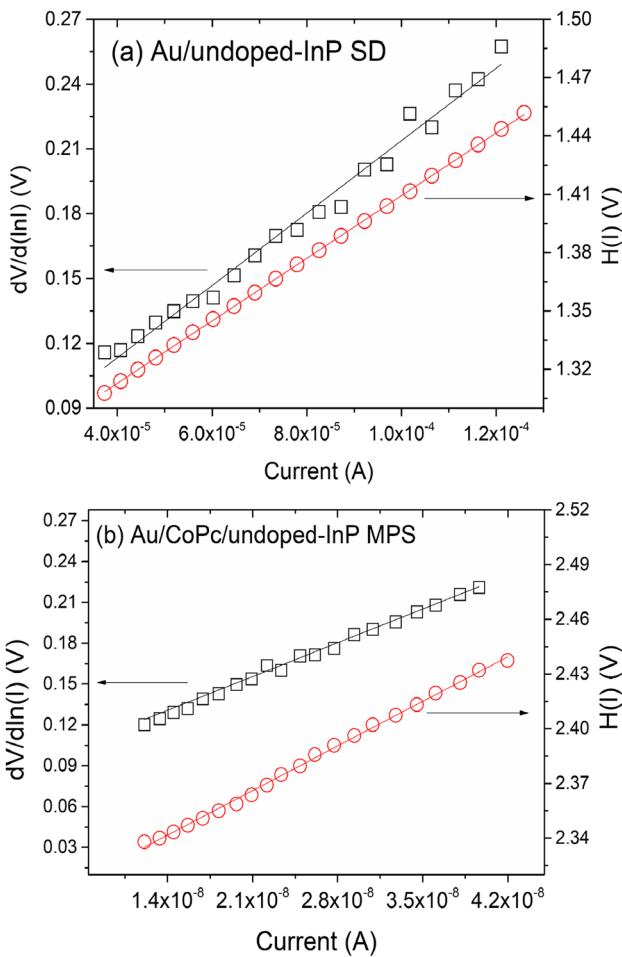
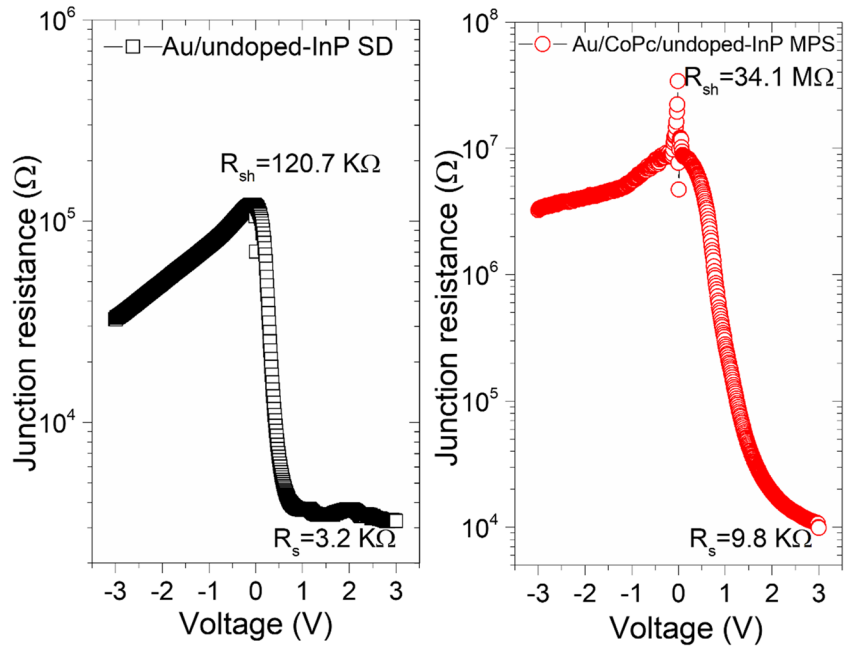


Fig. 6 Plot $dV/d(\ln I)$ versus I, and $H(I)$ versus I for the (a) Au/un-InP SD and (b) Au/CoPc/un-InP MPS diodes

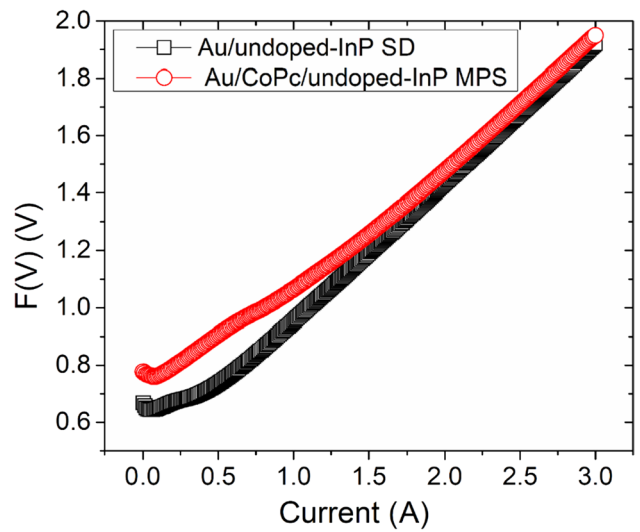


Fig. 7 Norde plot ($F(V)-V$) of the Au/un-InP SD and Au/CoPc/un-InP MPS diodes

The nonsaturation behavior of the I-V curves is perceived for both the SD and MPS diodes, which might be credited to generation-recombination, image force reduction and the existence of an interface layer [18, 41]. A reduced leakage current in the reverse bias is observed for the MPS diode (1.835×10^{-7} A at -1 V) compared to the SD (1.335×10^{-5} A at -1 V) which suggests that the electrical assets are enriched after the insertion of CoPc as an interlayer between the Au and un-InP semiconductor. The barrier height (Φ_B) and ideality factor (n) of the SD and MPS diodes are acquired based on the TE model [42].

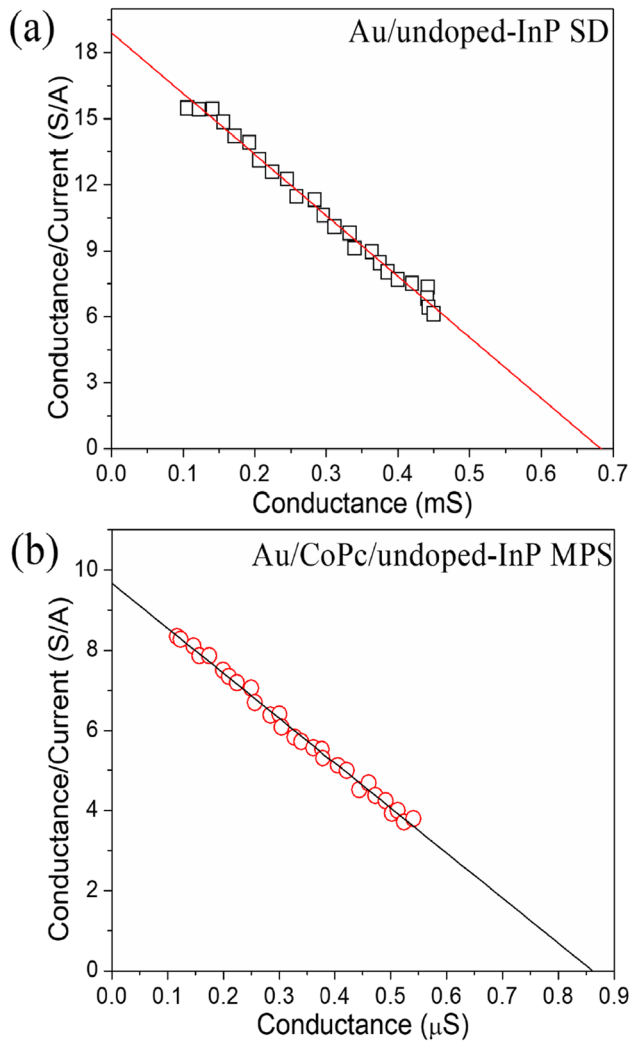


Fig. 8 Plot of G/I versus G for the (a) Au/un-InP SD and (b) Au/CoPc/un-InP MPS diodes

The derived magnitudes of Φ_B and n of the SD and MPS diode are 0.66 eV and 1.58, and 0.77 eV and 1.42, respectively. The results showed that Φ_B was more enhanced for the MPS diode than for the SD, indicating that the CoPc interlayer modifies Φ_B by altering the space charge at the CoPc-InP junction [13]. Thus, the CoPc film forms a real barrier that blocks the direct interface between the Au and the InP surface. Additionally, the CoPc interlayer drastically altered the InP's electron affinity and the metal's work function [13, 43]. A similar observation indicated that the increase in Φ_B of the MPS diode can allow the substrate band bend through the interlayer [9]. Our investigational findings indicate that the magnitude of deviation of ideality factor from unity for the SD and MPS diodes may be due to the existence of an excess current, a possible decrease in potential across the interfacial layer, and the incidence of series resistance and recombination current

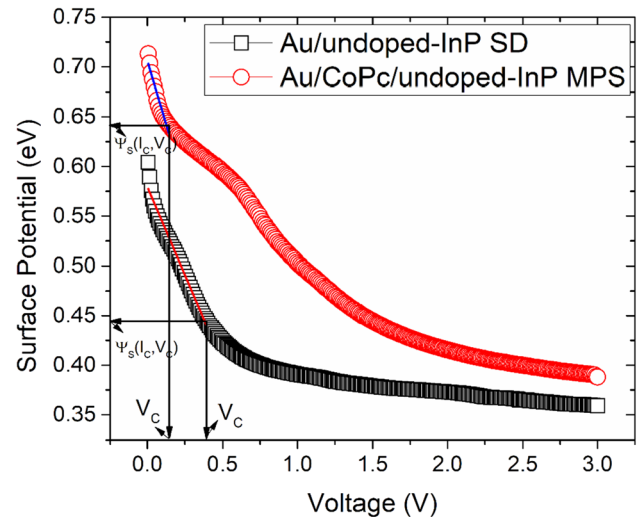


Fig. 9 Plot of Ψ_s versus forward-bias voltage for the Au/un-InP SD and Au/CoPc/un-InP MPS diodes

over the interface states at the junction [44]. Other reasons may include the inhomogeneous interface, uneven charge distribution at the interface, MIGS and voltage-dependent Φ_B at the interface [45, 46]. One more prospect may be due to the occurrence of secondary mechanisms inclusive of interface dipoles initiated via polymer interlayers or certain interface configurations, and to manufacture-caused flaws at the junction [47].

The performance and steadfastness of electronic devices depend strongly on the series resistance (R_S) and shunt resistance (R_{Sh}). Hence, it is imperative to evaluate the R_S and R_{Sh} of the SD and MPS diodes. Figure 5 elucidates the variation in R_j and the junction resistance with V for the SD and MPS diodes, from which the R_S and R_{Sh} are estimated. Mainly, a low R_S directs enhanced current transport across the junction, whereas a magnitude of R_{Sh} close to the edge indicates an insignificant leakage current across the junction. The magnitudes of R_S and R_{Sh} are determined from the plot (Fig. 5), in which, the lower part gives the R_S in the forward bias, while the maximum peak provides the R_{Sh} in the reverse bias. The R_S and R_{Sh} values are predicted to be 3.2 k Ω and 120.7 k Ω for the SD and 9.8 k Ω and 34.1 M Ω for the MPS diode, respectively.

It is noted that in the higher current section of the forward bias, the I-V curves deviate which is probably due to the R_S , density of states and presence of the interfacial layer. Thus, Φ_B , n and R_S are predicted in the higher current part of the I-V curves of the SD and MPS by using the method suggested by Cheung's [48] functions. Figure 6a and b illustrate the variations between $dV/d(\ln I)$ and I and between $H(I)$ and I for the SD and MPS diodes. The slope and y-axis intercept of the $dV/d(\ln I) - I$ plot (Fig. 6a and b) represent the R_S and n , and the analogous values are 1.67 k Ω and 1.79, and

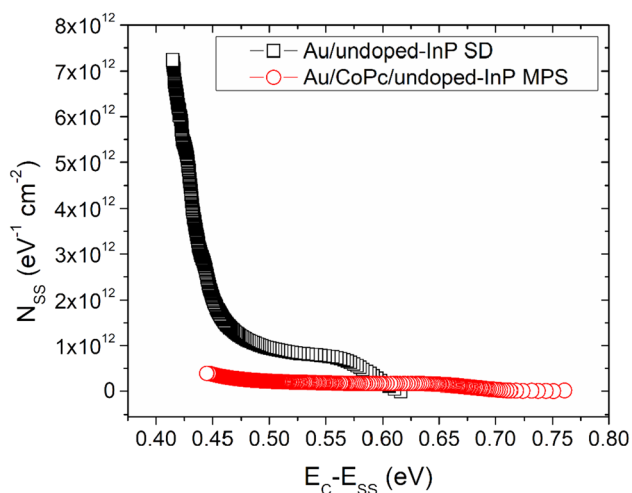


Fig. 10 N_{SS} versus $E_C - E_{SS}$ plot for the Au/un-InP SD and Au/CoPc/un-InP MPS diodes

3.54 MΩ and 3.13 for the SD and MPS, respectively. The slope and y-axis intercept of the $H(I) - I$ plot (Fig. 6a and b) represent the R_S and Φ_B , respectively, and the analogous values are 1.60 kΩ and 0.69 eV, and 3.49 MΩ and 0.73 eV for the SD and MPS diodes, respectively. The results indicate that the predicted R_S values from Cheung's plots are

well matched, which indicates that Cheung's derivations are trustworthy and expedient. Φ_B is closely matched with the value derived by way of the forward bias $\ln(I) - V$ plot. In contrast, the n estimated using the $dV/d(\ln I) - I$ plot differs to some extent from the value determined by the forward-bias $\ln(I) - V$ plot. This might be because the R_S and interface properties affect the I-V curves, but the R_S affects only the $dV/d(\ln I) - I$ plot [49, 50]. The modified Norde method [51] was also applied to obtain the Φ_B and R_S for the SD and MPS diodes. Figure 7 shows the Norde graph for the SD and MPS diodes, wherein, Φ_B and R_S are assessed. The predicted Φ_B and R_S values are 0.64 eV and 22 kΩ, 0.78 eV and 1.8 MΩ for the SD and MPS diodes, respectively. The findings reveal that the Φ_B values are similar to the values obtained with the aid of the I-V technique.

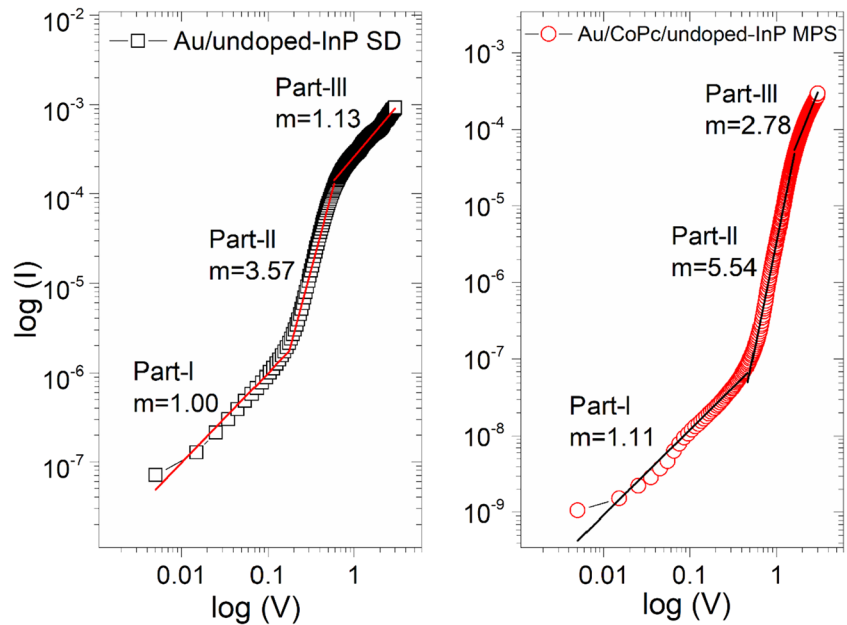
Werner proposed a simple method [52] to calculate the barrier parameters (R_S and n) from forward bias current-voltage characteristics of the contacts. Under forward bias conditions, the forward voltage ($V - IR_S$) is much greater than nkT/q , and the differential conductance (G) is defined as $G = dI/dV$. The diode current, based on the thermionic mechanism, can be expressed as

$$I = I_S \exp\left(\frac{\beta}{n} (V - IR_S)\right) \tag{1}$$

Table 1 The calculated various electronic parameters of the Au/un-InP SD and Au/CoPc/un-InP MPS

Parameters	Au/un-InP SD	Au/CoPc/un-InP MPS
I-V method		
Barrier height Φ_b (eV)	0.66	0.77
Ideality factor (n)	1.58	1.42
Series resistance (R_S)	3.2 kΩ	9.8 kΩ
Shunt resistance (R_{Sh})	120.7 kΩ	34.1 MΩ
Cheung's method		
$dV/d(\ln I)$ vs. I		
Ideality factor (n)	1.79	3.13
Series resistance (R_S)	1.67 kΩ	3.54 MΩ
$H(I)$ vs. I		
Barrier height Φ_b (eV)	0.69	0.73
Series resistance (R_S)	1.60 kΩ	3.49 MΩ
Norde method		
Barrier height Φ_b (eV)	0.64	0.78
Series resistance (R_S)	22 kΩ	1.8 MΩ
Werner method		
Ideality factor (n)	2.04	3.77
Series resistance (R_S)	1.47 kΩ	1.21 MΩ
Surface potential (Ψ_S)		
Barrier height Φ_b (eV)	0.64	0.77
Ideality factor (n)	2.84	1.98
Density of states (N_{SS}) ($eV^{-1} cm^{-2}$)		
	7.12×10^{12} to 3.91×10^{11}	4.42×10^9 to 2.19×10^{10}

Fig. 11 Plot of $\log(I)$ versus $\log(V)$ for the Au/un-InP SD and Au/CoPc/un-InP MPS diodes



The above equation yields the small signal conductance $G = \frac{dI}{dV}$,

$$\frac{G}{I} = \frac{\beta}{n} (1 - GR_S) \quad (2)$$

Further, a plot between G/I versus G can be used to analyze the device characteristics. Using Eq. (2), the plot of G/I versus G (shown in Fig. 8a and b) for the SD and MPS diodes yields a straight line that leads to the evaluation of $1/R_S$ and β/n from the x- and y-axis intercept, respectively. The straight line observed in Fig. 8a and b indicates the well-defined interfaces and good quality of the devices. Moreover, Werner's approach is effective in the voltage region where the effect of series resistance on the current is important. The determined R_S and n values are 1.47 k Ω and 2.04, and 1.22 M Ω and 3.77 for the SD and MPS diodes. These parameters were comparable to those evaluated by Cheung and Norde methods.

Considering the existence of an oxide layer on the semiconductor surface, the current generated via the MS junction may be stated by [42].

$$I = AA^*T^2 \exp\left(-\frac{q\Psi_S}{kT}\right) \left[-\frac{qV_p}{nkT}\right] \quad (3)$$

Here A^* , T , A , k , and n are typically defined as follows [18]. The critical surface potential $\Psi_S(I_C, V_C)$ and the critical voltage V_c are empirically identified, and the BH may be acquired. Ψ_S is the surface potential and is defined as [53].

$$\Psi_S = \frac{kT}{q} \ln \left[\frac{AA^*T^2}{I} \right] - V_p \quad (4)$$

Ψ_S is determined by using the value of V_p , and the V_p value is obtained using $V_p = \frac{kT}{q} \ln(N_v/N_a)$; now N_v and N_a usually have meanings [18]. The acquired Ψ_S values are contrary to the forward bias voltages for the SD and MPS diodes and are illustrated in Fig. 9. The critical surface potential $\Psi_S(I_c, V_c)$ and the critical voltage V_c are derived from the Ψ_S - V plot, so Φ_B is derived. Figure 9 demonstrates that the Ψ_S value decreases linearly until V reaches the critical value V_c . The BH is defined as

$$\Phi_B = \Psi_S(I_c, V_c) + \alpha V_c + V_p \quad (5)$$

Furthermore, quantity α is the converse of the ideality factor (n) and is defined as

$$-\alpha = \frac{1}{n} = \left(\frac{d\Psi_S}{dV} \right)_{I_c, V_c} \quad (6)$$

The Φ_B and n values are derived by Eqs. (5) and (6) for the SD and MPS diodes and the respective magnitudes are 0.64 eV and 2.84, and 0.77 eV and 1.98, respectively. The Φ_B magnitudes acquired from the forward-bias I-V data, Cheung's plots and Ψ_S - V curves are nearly the same, which suggests that the approaches employed here are consistent and reliable.

The density of states (N_{SS}) of the Au/un-InP SD and Au/CoPc/un-InP MPS diode is acquired from the forward bias I-V data based on $n(V)$ and Φ_e . The N_{SS} is defined as [54]

$$N_{SS} = \frac{1}{q} \left[\frac{\epsilon_i}{q} (n(V) - 1) - \frac{\epsilon_S}{W_D} \right] \quad (7)$$

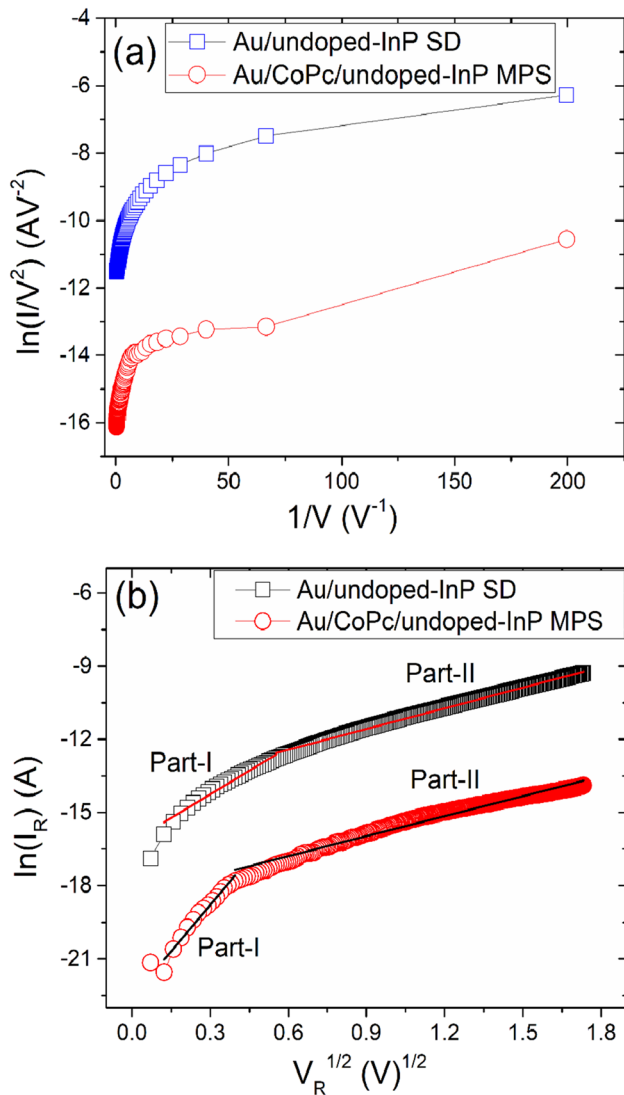


Fig. 12 (a) Plot of (a) $\ln(I/V^2)$ versus $1/V$ and (b) Plot of $\ln(I_R)$ versus $V^{1/2}$ for the Au/un-InP SD and Au/CoPc/un-InP MPS diodes

Here W_d , ϵ_s , ϵ_i , δ and $n(V)$ are usually defined [18], and nV can be defined as $n(V) = (q/kT)[V/(\ln(I/I_0))]$. In an n-type semiconductor, the energy of interface states (E_{SS}) concerning the lowest of the conduction band at the surface of the semiconductor is stated by

$$E_C - E_{SS} = q(\Phi_e - V) \quad (8)$$

Φ_e is defined by

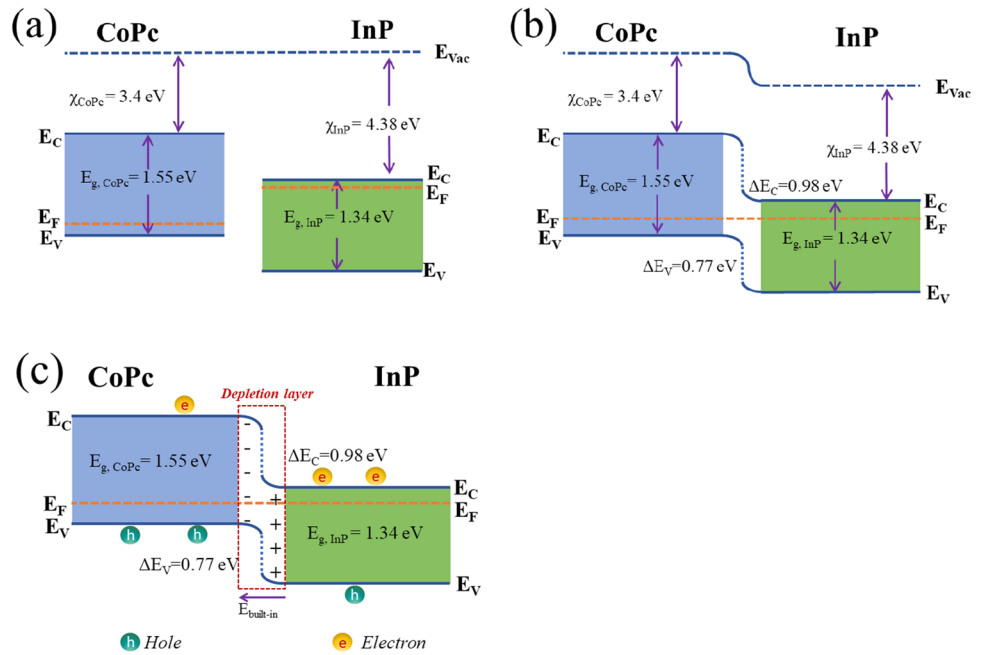
$$\Phi_e = \Phi_b + \beta V, \text{ where } \frac{d\Phi_e}{dV} = \beta = 1 - \frac{1}{n(V)} \quad (9)$$

Figure 10 shows the variation in the N_{SS} with $E_C - E_{SS}$ for the SD and MPS diodes, wherein, the N_{SS} magnitudes (Fig. 10) decrease with increasing $E_C - E_{SS}$. The derived

N_{SS} magnitudes are in the range of $7.12 \times 10^{12} \text{ eV}^{-1} \text{ cm}^{-2}$ to $3.91 \times 10^{11} \text{ eV}^{-1} \text{ cm}^{-2}$ for the SD and $4.42 \times 10^9 \text{ eV}^{-1} \text{ cm}^{-2}$ to $2.19 \times 10^{10} \text{ eV}^{-1} \text{ cm}^{-2}$ for the MPS diodes. The N_{SS} magnitude acquired for the MPS diode is less than the value acquired for the SD, implying that the InP surface is effectively passivated by the CoPc layer and, consequently the lower N_{SS} . The findings indicated that the CoPc interlayer results in tremendous adjustments in the interfacial states, although the polymer/un-InP interface appears to be abrupt and unreactive [15, 16]. The results suggest that the CoPc layer plays a generous role in decreasing N_{SS} and enriching the Φ_e of the SD. The determined Φ_B , n , R_S and N_{SS} values of the SD and MPS diodes are summarized in Table 1.

The thermionic emission mechanism is applied in a Schottky contact to model the current–voltage properties in the evaluation of barrier parameters such as barrier height and ideality factor for forward voltage $V < 3kT/q$. On the other hand, the $\log I$ vs. $\log V$ graph of the diodes provides insight into the conduction properties that are directly related to the space charges present at the junction. These properties depend greatly on the mobility of the carriers, bias potential, and traps that are present at the junction [55, 56]. To explore the forward current conduction processes in the SD and MPS diodes, $\log I$ versus $\log V$ are plotted and illustrated in Fig. 11, where three different linear regions are noted (labeled as part-I, part-II and part-III) and every slope has its value that follows the $I \propto V^m$ relation (here, m is the power exponent, and the slope of the linear section of each part provides the m value, i.e., the current is proportionate to the applied bias). For the SD and MPS diodes, the m values are estimated to be 1.00, 3.57, 1.13 and 1.11, 5.54, 2.78 in parts I, II and III, respectively. Seemingly, in the lower-bias section (part-I), the current conduction shows ohmic properties for both the SD and MPS diodes. The value of 'm' close to 1 indicates a possible linear relationship between voltage and current due to thermally generated carriers [57–59]. The I–V correlation may be described by way of the power law dependence. In part-II, the slope values are greater than 2 for both the SD and MPS diodes, which could be inferred as a trap-charge limiting current process (TCLC) with traps distributed exponentially [18, 23, 60]. Thus, an increased density of injected electrons leads to the filling of traps and the escalation of space charges [23, 61]. Additionally, the slope values of the SD and MPS diode gradients decrease in the upper-bias section (part-III) as junctions reach the trap-filled limit. As a result, electrons escape the trap because of the sturdy injection of electrons and give rise to the SCLC. The findings exhibit a coherent transformation from an ohmic-type conduction at the lower-bias section (part-I) to an SCLC at the upper-bias section (part-II and part-III) for both the SD and MPS diodes. However, the thermionic emission currents and space charge limited emission currents are always competing transport processes in Schottky contacts.

Fig. 13 Schematic energy band diagrams of the CoPc/InP structure (a) before contact, (b) after contact, and (c) under dark conditions



To analyze the reverse current transport mechanisms in the SD and MPS diodes, Fowler–Nordheim (FN), Poole–Frenkel emission (PFE) and Schottky emission (SE) are considered via the interface. However, numerous conduction processes might also arise at specific applied voltages. As a result, it is challenging to comprehend entirely and assess the reliable current transport process for the FN, PFE and SE. The current is ruled by the FN across the junction and is defined as [18, 62–64].

$$I_{\text{FN}} = AV^2 \exp\left(-\frac{B}{V}\right), \text{ where } A = \frac{q^3 m}{8\pi m^* \Phi_b}, B = 8\pi(q\Phi_b)^3 / 3qh \quad (10)$$

Here q , h and m^* are common denotations [18]. The plot of $\ln(I/V^2)$ versus $1/V$ for the SD and MPS diodes is depicted in Fig. 12a. The plot reveals a linear curve with a positive slope. As stated by Eq. (10), the slope must be negative; and consequently, the impact of FN tunneling is probably a constrained conduction process in both the SD and MPS diodes. The reverse current is governed by the PFE and is described by [63, 64].

$$I_{\text{R}} = I_0 \exp\left(\frac{\beta_{\text{PF}} V^{1/2}}{kTd^{1/2}}\right) \quad (11)$$

and for the SE

$$I_{\text{R}} = AA^* T^2 \exp\left(-\frac{\Phi_s}{kT}\right) \exp\left(\frac{\beta_{\text{SC}} V^{1/2}}{kTd^{1/2}}\right) \quad (12)$$

Here d is the depletion width, β_{PF} is the PFE and β_{SC} is the SE lowering constant. The hypothetical values for β_{PF} and β_{SC} are given by

$$2\beta_{\text{SC}} = \beta_{\text{PF}} = \left(\frac{q^3}{\pi\epsilon_0\epsilon_r}\right)^{1/2} \quad (13)$$

Using Eq. (13), the hypothetical values for β_{PF} and β_{SC} are acquired, the values are $2.15 \times 10^{-5} \text{ eVm}^{1/2}\text{V}^{-1/2}$ and $1.07 \times 10^{-5} \text{ eVm}^{1/2}\text{V}^{-1/2}$ for the SD, and $4.05 \times 10^{-5} \text{ eVm}^{1/2}\text{V}^{-1/2}$ and $2.02 \times 10^{-5} \text{ eVm}^{1/2}\text{V}^{-1/2}$ for the MPS diode, respectively. A $\ln(I_{\text{R}})$ versus $V_{\text{R}}^{1/2}$ graph plotted for the SD and MPS diodes is presented in Fig. 12b. As shown in Fig. 12b, there are two different straight regions (labeled as part-I and part-II) for the SD and MPS diodes, where the observed magnitudes of the slopes are $2.88 \times 10^{-5} \text{ eVm}^{1/2}\text{V}^{-1/2}$ and $1.26 \times 10^{-5} \text{ eVm}^{1/2}\text{V}^{-1/2}$ for the SD and $5.58 \times 10^{-5} \text{ eVm}^{1/2}\text{V}^{-1/2}$ and $1.41 \times 10^{-5} \text{ eVm}^{1/2}\text{V}^{-1/2}$ for the MPS diode in part-I and part-II, respectively. In part-I, the slope magnitudes are well coordinated with the hypothetical magnitudes of β_{PF} ; hence, PFE is dominant in the reverse leakage current in the lower-bias section for both the SD and MPS diodes. Although the slope values in part-II nearly concur with the hypothetical values of β_{SC} , the SE has ruled the reverse leakage current in the higher-bias section for both the SD and MPS diodes. Due to the nonuniformity and subatomic structure of the CoPc layer, reverse current conduction occurs over the contact interface in the SE instead of from the bulk material [18, 65]. In the case of PFE, the occurrence of a large density of structural defects or trap levels in the CoPc film can account for the increased concert of trapped/detrapped charge carriers [14, 18]. Figure 13 shows the energy band diagrams of the CoPc/InP structure before contact, after contact, and under dark conditions.

4 Conclusions

In this work, first, cobalt phthalocyanine (CoPc) films were thermally deposited on an un-InP substrate and their chemical, structural and morphological properties were probed via XPS, Raman and AFM approaches. Raman measurements of the phthalocyanine thin films revealed dominant characteristic vibrational bands at 1537 cm^{-1} , indicating the crystalline quality of the films. XPS results confirmed that the CoPc film was formed on the un-InP surface. Then, the Au/CoPc/un-InP MPS diode and Au/un-InP SD were fabricated, and their electrical properties were examined via the I-V technique. The derived barrier heights (Φ_B) were 0.66 eV and 0.77 eV for the SD and MPS diodes, respectively. An increase in Φ_B was observed for MPS compared with SD, implying that Φ_B was modified by using a thin CoPc interlayer. The BHs were also derived through Cheung's, and Norde methods, and the Ψ_s -V curves are almost equal to the values derived from the I-V data, which indicates that the methods implemented here are trustworthy and effective. The Rs of the SD and MPS diodes were derived by the I-V, Cheung, and Norde methods and the corresponding magnitudes are analogous. The results confirmed that the expected N_{SS} was lower for the MPS diode than for the SD, suggesting that the CoPc layer plays a generous role in decreasing the N_{SS} . For the SD and MPS, the forward current conduction process was ruled out by the ohmic nature and SCLC in the lower-bias and higher-bias sections. The reverse leakage current is directed by the PFE in the lower-bias section, while, the SE is governed in the higher-bias section for both the SD and MPS diodes. The results revealed that the CoPc layer is a potential material for the development of organic-inorganic electronic devices.

Author Contributions AUR: all the experimental work and writing-original draft. VRR: reviewing and editing. CVP: data interpretation. AAK: structural analysis.

Funding The authors have not disclosed any funding.

Data Availability No datasets were generated or analysed during the current study.

Declarations

Competing Interests The authors declare no competing interests.

References

- G. Lloyd, M. Raja, I. Sellers, N. Sedghi, R. Di Lucrezia, S. Higgins, B. Eccleston, The properties of MOS structures using conjugated polymers as the semiconductor. *Microelectron. Eng.* **59**, 323–328 (2001)
- M. Zhu, T.H. Cui, K. Varahramyan, Experimental and theoretical investigation of MEH-ppv based Schottky diodes. *Microelectron. Eng.* **75**, 269–274 (2004)
- S.A. Moiz, M.M. Ahmed, K.S. Karimov, Estimation of electrical parameters of OD organic semiconductor diode from measured I-V characteristics. *ETRI J.* **27**, 319–325 (2005)
- M.E. Aydin, A. Turut, The electrical characteristics of Sn/methyl-red/p-type Si/Al contacts. *Microelectron. Eng.* **84**, 2875–2882 (2007)
- W.-C. Huang, T.-F. Lie, C.-L. Lee, A double metal structure Pt/Al/n-InP diode. *J. Appl. Phys.* **78**, 291–294 (1995)
- O. Gullu, O. Baris, M. Biber, A. Turut, Laterally inhomogeneous barrier analysis of the methyl violet/p-Si organic/inorganic hybrid Schottky structures. *Appl. Surf. Sci.* **254**, 3039–3044 (2008)
- M.D. Aydin, F. Yakuphanoglu, Molecular control over Ag/p-Si diode by organic layer. *J. Phys. Chem. Solids* **68**, 1770–1773 (2007)
- M.M. El-Nahass, K.F. Abd-El-Rahman, A.A.M. Farag, A.A.A. Darwish, Photovoltaic properties of NiPc/p-Si (organic/inorganic) heterojunctions. *Org. Electron.* **6**, 129–136 (2005)
- A.R. Vearey-Roberts, D.A. Evans, Modification of GaAs Schottky diodes by thin organic interlayers. *Appl. Phys. Lett.* **86**, 072105 (2005)
- O. Gullu, Ultrahigh (100%) barrier modification of n-InP Schottky diode by DNA biopolymer nanofilms. *Microelectron. Eng.* **87**, 648–651 (2010)
- J. Jortner, M.A. Ratner, *Molecular electronics* (American Chemical Society, Washington, 1997)
- M. Siva Pratap Reddy, H.-S. Kang, J.-H. Lee, V. Rajagopal Reddy, J.-S. Jang, Electrical properties and the role of inhomogeneities at the polyvinyl alcohol/n-InP Schottky barrier interface. *J. Appl. Polym. Sci.* **131**, 39773 (2014)
- V. Rajagopal Reddy, Electrical properties of Au/polyvinylidene fluoride/n-InP Schottky diode with polymer interlayer. *Thin Solid Films* **556**, 300–306 (2014)
- P.R. Sekhar Reddy, V. Janardhanam, I. Jyothi, S.-H. Yuk, V. Rajagopal Reddy, J.-C. Jeong, S.-N. Lee, C.-J. Choi, Modification of Schottky barrier properties of Ti/p-type InP Schottky diode by polyaniline (PANI) organic interlayer. *J. Semicond. Technol. Sci.* **16**, 664–674 (2016)
- K. Sreenu, C. Venkata Prasad, V. Rajagopal Reddy, Barrier parameters and current transport characteristics of Ti/p-InP Schottky junction modified using orange G (OG) organic interlayer. *J. Electron. Mater.* **46**, 5746–5754 (2017)
- M. Siva Pratap Reddy, K. Sreenu, V. Rajagopal Reddy, C. Park, Modified electrical properties and transport mechanism of Ti/p-InP Schottky structure with a polyvinylpyrrolidone (PVP) polymer interlayer. *J. Mater. Sci. Mater. Electron.* **28**, 4847–4855 (2017)
- P.R. Sekhar Reddy, V. Janardhanam, I. Jyothi, C.S. Harsha, V. Rajagopal Reddy, S.-N. Lee, J. Won, C.-J. Choi, Effect of copper phthalocyanine thickness on surface morphology, optical and electrical properties of Au/CuPc/n-Si heterojunction. *Appl. Phys. A* **124**, 115 (2018)
- V. Rajagopal Reddy, C. Venkata Prasad, K. Ravindranatha Reddy, Chemical, electrical and carrier transport properties of Au/cytosine/undoped-InP MPS junction with a cytosine polymer. *Solid State Sci.* **97**, 105987 (2019)
- A. Tataroglu, S. Altundal, Y. Azizian-Kalendaragh, C-V-f and G/ ω -V-f characteristics of Au/(In₂O₃-PVP)/n-Si (MPS) structure. *Phys. B* **582**, 11996 (2020)
- E.E. Baydilli, S.O. Tan, H.U. Tecimer, S. Altundal, Detection of current transport mechanisms for graphene-doped-PVA interlayered metal/semiconductor structures. *Phys. B* **598**, 412457 (2020)
- Y. Azizian-Kalendaragh, I. Yucedag, G. Ersoz Demir, S. Altundal, Investigation of the variation of dielectric properties by applying frequency and voltage to Al/(CdS-PVA)/p-Si structures. *J. Mol. Struc.* **1224**, 129325 (2021)
- S. Demirezen, H.G. Cetinkaya, M. Kara, F. Yakuphanoglu, S. Altundal, Synthesis, electrical and photosensing characteristics of the Al/(PCBM/NiO:ZnO)/p-Si nanocomposite structures. *Sens. Actuators A* **317**, 112449 (2021)

23. V. Rajagopal Reddy, C. Venkata Prasad, V. Janardhanam, C.-J. Choi, Electrical and carrier transport properties of Ti/ α -amylase/p-InP MPS junction with a α -amylase polymer interlayer. *J. Mater. Sci. Mater. Electron.* **32**, 8092–8105 (2021)
24. S. Altındal, Y. Azizian-Kalandaragh, M. Ulusoy, G. Pirgholi-Givi, The illumination effects on the current conduction mechanisms of the Au/(Er₂O₃:PVC)/n-Si (MPS) Schottky diodes. *J. Appl. Polym. Sci.* **139**, 52497 (2022)
25. O. Gullu, S. Aydogan, A. Turut, High barrier Schottky diode with organic interlayer. *Solid State Commun.* **152**, 381–385 (2012)
26. K.M. Al-Adamat, H.M. El-Nasser, Characterization of cobalt phthalocyanine thin film on silicon substrate using spectroscopic ellipsometry. *Ukr. J. Phys.* **66**, 562–569 (2021)
27. P.-C. Kao, S.-Y. Chu, Z.-X. You, S.J. Liou, C.-A. Chuang, Improved efficiency of organic light-emitting diodes using CoPc buffer layer. *Thin Solid Films* **498**, 249–253 (2006)
28. M. Szybowicz, W. Bała, K. Fabisiak, K. Paprocki, M. Drozdowski, The molecular structure ordering and orientation of the metallophthalocyanine CoPc, ZnPc, CuPc, and MgPc thin layers deposited on silicon substrate, as studied by micro-Raman spectroscopy. *J. Mater. Sci.* **46**, 6589–6595 (2011)
29. P. Popielarski, W. Bala, K. Paprocki, L. Mosinska, M. Kowalska, M. Szybowicz, J. Makowiecki, Admittance spectroscopy of CuPc-Si and CoPc-Si heterostructures. *Electrochim. Acta* **104**, 496–504 (2013)
30. M. Braik, C. Dridi, M. Ben Ali, A. Ali, M.N. Abbas, A. Errachid, Investigation of structural, optical and electrical properties of a new cobalt phthalocyanine thin films with potential applications in perchlorate sensor. *Synth. Met.* **209**, 135–142 (2015)
31. D. Guo, J. Zhang, G. Liu, X. Luo, F. Wu, Cobalt phthalocyanine-based nanodots as efficient catalysts for chemical conversion of CO₂ under ambient conditions. *J. Mater. Sci.* **56**, 10990–10999 (2021)
32. H. Zhang, S. Min, F. Wang, Z. Zhang, Immobilizing cobalt phthalocyanine into a porous carbonized wood membrane as a self-supported heterogenous electrode for selective and stable CO₂ electroreduction in water. *Dalton Trans.* **49**, 15607–15611 (2020)
33. L. Zhao, Z. Lan, W. Mo, C. Zhang, Co/Co₂N/N/C oxygen reduction reaction catalysts derived from sisal fiber porous carbon and cobalt phthalocyanine. *Mater. Lett.* **338**, 134062 (2023)
34. J. Liu, H.-Y. Yu, T.-H. Zhang, W.-T. Wang, X.-F. Han, Y.-X. Yuan, J.-L. Yao, R. Yang, J.-H. Tian, Honeycomb-like self-supported Co–N–C catalysts with an ultrastable structure: highly efficient electrocatalysts toward oxygen reduction reaction in alkaline and acidic solutions. *ACS Appl. Energy Mater.* **4**, 2522–2530 (2021)
35. S. Wang, P. Sun, N. Li, J. Wang, L. Zhang, W. Duan, S. Li, The catalytic performance enhanced via π -electron cloud interaction of polymerized cobalt phthalocyanine/3D-graphene as bifunctional oxygen catalysts for Zn-air battery. *J. Power. Sources* **556**, 232471 (2023)
36. P. Kumar, A. Kumar, B. Sreedhar, B. Sain, S.S. Ray, S.L. Jain, Cobalt phthalocyanine immobilized on graphene oxide: an efficient visible-active catalyst for the photoreduction of carbon dioxide. *Chem. Eur. J.* **20**, 6154–6161 (2014)
37. W. Huang, J. Li, X. Xu, A. Cao, Y. He, M. Sun, L. Kang, Controllable dispersion of cobalt phthalocyanine molecules on graphene oxide for enhanced electrocatalytic reduction of CO₂ to CO. *New J. Chem.* **46**, 7153–7160 (2022)
38. S.I. Dorovskikh, D.D. Klyamer, E.A. Maksimovskiy, V.V. Volchek, S.M. Zharkov, N.B. Morozova, T.V. Basova, Heterostructures based on cobalt phthalocyanine films decorated with gold nanoparticles for the detection of low concentrations of ammonia and nitric oxide. *Biosensors* **12**, 476 (2022)
39. K.H. Do, D.P. Kumar, A.P. Rangappa, Y. Hong, D.A. Reddy, T.K. Kim, Indium phosphide quantum dots integrated with cadmium sulfide nanorods for photocatalytic carbon dioxide reduction. *ChemCatChem* **12**, 4550–4557 (2020)
40. N. Balaram, M.S.P. Reddy, V.R. Reddy, C. Park, Effects of high-k zirconium oxide (ZrO₂) interlayer on the electrical and transport properties of Au/n-type InP Schottky diode. *Thin Solid Films* **619**, 231–238 (2016)
41. M. Yalcin, D. Ozmen, F. Yakuphanoglu, Perovskite cobaltates/p-silicon heterojunction photodiodes. *J. Alloys Compd.* **796**, 243–254 (2019)
42. E.H. Rhoderick, R.H. Williams, *Metal-semiconductor contacts*, 2nd edn. (Clarendon, Oxford, 1988)
43. M. Cakar, C. Temirci, A. Turut, The Schottky barrier height of the rectifying Cu/pyronine-B/p-Si, Au/pyronine-B/p-Si, Sn/pyronine-B/p-Si and Al/pyronine-B/p-Si contacts. *Synth. Met.* **142**, 177–180 (2004)
44. A.A.M. Farag, Structure and transport mechanisms of Si/porous Si n-p junctions prepared by liquid phase epitaxy. *Appl. Surf. Sci.* **255**, 3493–3498 (2009)
45. R.T. Tung, Electron transport at metal-semiconductor interfaces: general theory. *Phys. Rev. B Condens. Matter* **45**, 13509–13523 (1992)
46. H. Cetin, B. Sahin, E. Ayyildiz, A. Turut, Ti/p-Si Schottky barrier diodes with interfacial layer prepared by thermal oxidation. *Phys. B: Condens. Matter.* **364**, 133–141 (2005)
47. W. Monch, Barrier heights of real Schottky contacts explained by metal-induced gap states and lateral inhomogeneities. *J. Vac. Sci. Technol. B* **17**, 1867–1876 (1999)
48. S.K. Cheung, N.W. Cheung, Extraction of Schottky diode parameters from forward current-voltage characteristics. *Appl. Phys. Lett.* **49**, 85–87 (1986)
49. C. Bilkan, Y. Azizian-Kalandaragh, O. Sevgili, S. Altındal, Investigation of the efficiencies of the (SnO₂-PVA) interlayer in Au/n-Si (MS) SDs on electrical characteristics at room temperature by comparison. *J. Mater. Sci. Mater. Electron.* **30**, 20479–20488 (2019)
50. P. Prabhu Thapaswini, R. Padma, N. Balaram, B. Bindu, V. Rajagopal Reddy, Modification of electrical properties of Au/n-type InP Schottky diode with a high-k Ba_{0.6}Sr_{0.4}TiO₃ interlayer. *Superlattices Microstruct.* **93**, 82–91 (2016)
51. H. Norde, A modified forward I-V plot for Schottky diodes with high series resistance. *J. Appl. Phys.* **50**, 5052–5053 (1979)
52. J.H. Werner, Schottky barrier and pn-junction I/V plots-small signal evaluation. *Appl. Phys. A* **47**, 291–300 (1988)
53. P. Chattopadhyay, A new technique for the determination of barrier height of Schottky barrier diodes. *Solid State Electron.* **38**, 739–741 (1995)
54. E.H. Rhoderick, H.C. Card, Studies of tunnel MOS diodes I. Interface effects in silicon Schottky diodes. *J. Phys. D: Appl. Phys.* **4**, 1589–1601 (1971)
55. I. Pandurangavali, P. Kumara Shetty, M.G. Mahesha, V.C. Petwal, J. Dwivedi, R.J. Choudhary, Tuning of Schottky barrier height of Al/n-Si by electron beam irradiation. *Appl. Surf. Sci.* **407**, 171–176 (2017)
56. S. Aydogan, K. Cinar, H. Asil, C. Coskun, A. Turut, Electrical characterization of Au/n-ZnO Schottky contacts on n-Si. *J. Alloys Compd.* **476**, 913–918 (2009)
57. S. Alptekin, S. Altındal, A comparative study on current/capacitance: voltage characteristics of Au/n-Si (MS) structures with and without PVP interlayer. *J. Mater. Sci. Mater. Electron.* **30**, 6491–6499 (2019)
58. S. Altındal, O. Sevgili, Y. Azizian-Kalandaragh, A comparison of electrical parameters of Au/n-Si and Au/(CoSO₄-PVP)/n-Si structures (SBDs) to determine the effect of (CoSO₄-PVP) organic interlayer at room temperature. *J. Mater. Sci. Mater. Electron.* **30**, 9273–9280 (2019)
59. A. Tataroğlu, S. Altındal, Y. Azizian-Kalandaragh, Comparison of electrical properties of MS and MPS type diode in respect of (In₂O₃-PVP) interlayer. *Phys. B: Condens. Matter.* **576**, 411733 (2020)
60. I. Tascioglu, U. Aydemir, S. Altındal, The explanation of barrier height inhomogeneities in Au/n-Si Schottky barrier diodes with organic thin interfacial layer. *J. Appl. Phys.* **108**, 064506 (2010)

61. Y.S. Ocak, M. Kulakci, T. Kilicoglu, R. Turan, K. Akkılıc, Current-voltage and capacitance-voltage characteristics of a Sn/methylene blue/p-Si Schottky diode. *Synth. Met.* **159**, 1603–1607 (2009)
62. M. Leczilinger, E.H. Snow, Fowler-Nordheim tunneling into thermally grown SiO₂. *J. Appl. Phys.* **40**, 278–283 (1969)
63. M. Gulnazar, T. Karacali, H. Efeoglu, Characterization of electrical transport and properties of an Al/porous Si (PS)/p-Si/Al heterojunction. *J. Alloys Compd.* **797**, 859–864 (2019)
64. M. Gulnazar, T. Karacali, H. Efeoglu, Porous Si based Al Schottky structures on p⁺-Si: a possible way for nano Schottky fabrication. *Electrochim. Acta* **168**, 41–49 (2015)
65. A.C. Varghese, C.S. Menon, Electrical properties of hybrid phthalocyanines thin films using gold and lead electrodes. *Eur. Phys. J. B.* **47**, 485–489 (2005)

Publisher's Note Springer Nature remains neutral with regard to jurisdictional claims in published maps and institutional affiliations.

Springer Nature or its licensor (e.g. a society or other partner) holds exclusive rights to this article under a publishing agreement with the author(s) or other rightsholder(s); author self-archiving of the accepted manuscript version of this article is solely governed by the terms of such publishing agreement and applicable law.